Invited Paper

Quantum enhancement of a coherent LADAR receiver using phase-sensitive amplification

Peter A. Wasilousky[a], Kevin H. Smith*[a], Ryan Glasser[a], Geoffrey L. Burdge[a], Lee Burberry[a], Bill Deibner[a], Michael Silver[a], Robert C. Peach[a], Christopher Visone[a], Prem Kumar[b], Oo-Kaw Lim[b], Gideon Alon[b], Chao-Hsiang Chen[b], Amar R. Bhagwat[b], Paritosh Manurkar[b], Michael Vasilyev[c], Muthiah Annamalia[c], Nikolai Stelmakh[c], Zachary Dutton[d], Saikat Guha[d], Cesar Santivañez[d], Jian Chen[d], Marcus Silva[d], Will Kelly[d], Jeffrey H. Shapiro[e], Ranjith Nair[e], Brent J. Yen[e], Franco N. C. Wong[e]

[a]Harris Corporation GCSD, PO Box 37 MS 13-11A, Melbourne, FL, USA 32902-0037; [b]Center for Photonic Communication and Computing, EECS Department, Northwestern University, 2145 Sheridan Road, Evanston, IL 60208; [c]Dept. of Electrical Engineering, University of Texas at Arlington, Arlington, TX 76019; [d]Raytheon BBN Technologies, 10 Moulton St., Cambridge, MA 02138; [e]Research Laboratory of Electronics, Massachusetts Institute of Technology, Cambridge, MA 02139

ABSTRACT

We demonstrate a balanced-homodyne LADAR receiver employing a phase-sensitive amplifier (PSA) to raise the effective photon detection efficiency (PDE) to nearly 100%. Since typical LADAR receivers suffer from losses in the receive optical train that routinely limit overall PDE to less than 50% thus degrading SNR, PSA can provide significant improvement through amplification with noise figure near 0 dB. Receiver inefficiencies arise from sub-unity quantum efficiency, array fill factors, signal-local oscillator mixing efficiency (in coherent receivers), etc. The quantum-enhanced LADAR receiver described herein is employed in target discrimination scenarios as well as in imaging applications. We present results showing the improvement in detection performance achieved with a PSA, and discuss the performance advantage when compared to the use of a phase-insensitive amplifier, which cannot amplify noiselessly.

Keywords: LADAR, coherent detection, phase-sensitive amplification, balanced homodyne detection, heterodyne LADAR

1. INTRODUCTION

1.1 DARPA Quantum Sensors Program

In the following discussion, we present results from one activity performed on the second phase of a DARPA directed Quantum Sensors Program (QSP) effort aimed at demonstrating tangible improvements in coherent LADAR receiver performance using non-classical quantum properties of light. Under an earlier Phase I study portion of the program it was determined that among a variety of quantum-enhanced sensor modalities, a sensor utilizing classical light to illuminate the target in conjunction with a non-standard receiver employing an advanced Quantum Image Enhancer (QIE), showed the most promise for achieving improvements in detection performance in high signal-loss operational scenarios. The QIE would be inserted between the receive optics and the detector of a classical homodyne receiver and be comprised of two elements, a squeezed vacuum injector (SVI) that would restore the high spatial frequencies lost by attenuation in soft aperture entrance optics, and a phase-sensitive amplifier (PSA) that overcomes the inefficiency of the homodyne detector[1]. Here we address implementation and performance aspects related to use of the PSA element in an operational standoff coherent LADAR receiver.

*ksmith35@harris.com; phone 321-727-4936; www.harris.com

Quantum Communications and Quantum Imaging IX, edited by
Ronald E. Meyers, Yanhua Shih, Keith S. Deacon, Proc. of SPIE Vol. 8163,
816305 · © 2011 SPIE · CCC code: 0277-786X/11/$18 · doi: 10.1117/12.892419

LADAR systems are currently deployed in 3D mapping and target identification applications. Improvement of the SNR performance of a LADAR receiver results directly in an enhanced capability to resolve features and to distinguish and identify targets. This paper describes the breadboard quantum-enhanced LADAR system built at Harris Corporation in three parts. Section 2 covers the design and calibration of a baseline coherent LADAR system with no quantum enhancements. Section 3 describes the enhancement of this baseline system through the insertion of a phase-locked PSA into the receive train, and Section 4 provides experimental verification of the improvements afforded by the PSA. Section 5 presents a brief summary of the results of this work.

2. BASELINE LADAR

The current Phase II QSP Program represents a collaborative effort between several industry and academic partners to explore various related quantum effects for use in optical receiver applications. One activity associated with the Phase II effort involved the development of a suitable standoff LADAR to assess the efficacy of a PSA when utilized as an optimal preamplifier to compensate for various PDE losses in the receiver. This baseline LADAR (without quantum enhancements) forms the reference against which improvements in performance could be measured. In the following section, we present a brief overview of the baseline LADAR configuration along with data characterizing the receiver sensitivity, and slant and cross range resolution at high SNR operation.

2.1 Baseline LADAR Implementation

To facilitate the development effort, the baseline coherent LADAR receiver was configured from readily available commercial optical and electrical components. In some instances, custom versions were procured to assure the required pump power levels could be generated to support parametric optical amplification using a PPLN crystal as the relevant PSA element. Figure 1 shows many of the key components used in the development of the baseline LADAR. A Model 2117 balanced InGaAs detector from New Focus was used as the core element in the balanced interferometer-based heterodyne optical receiver. To meet the narrow optical linewidth necessary to support coherent standoff detection, a 1560 nm Orbits Lightwave virtual ring laser with extremely narrow linewidth and low phase noise was employed as the optical source. To support the ability to obtain slant range, as well as the generation of high peak pulse powers required for optical amplification, a custom-designed pulse carver utilizing a high extinction EOSpace modulator was designed and assembled. Finally, two high performance optical amplifiers were cascaded to amplify the pulse carved output for use as a subsequent target illumination, local oscillator (LO), and frequency-doubled PSA pump source. To support cross-range imaging, a high-precision, dual-axis, scan mirror was used to direct the target return to the receiver scan optics. Both image and detection processing, along with system control functions for directing the mirror position and coordinating the slant range pulse timing, were handled by PXI-based hardware from National Instruments.

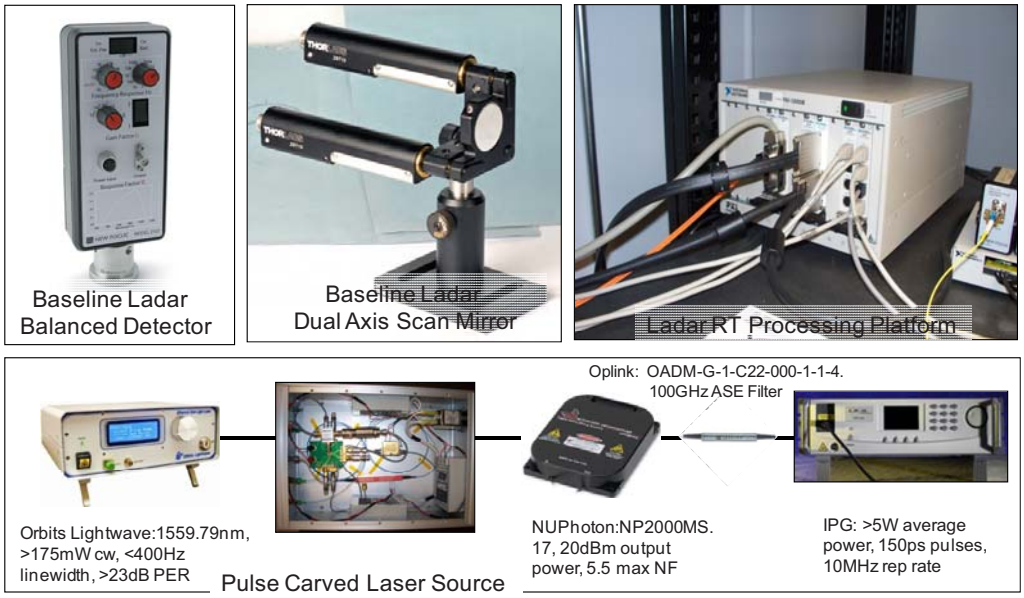

Figure 1. Baseline LADAR critical components.

Before introducing the PSA, it was necessary to characterize the performance of the baseline LADAR both in terms of its noise and sensitivity, as well as operational performance with regard to cross- and slant-range resolution. While characterization of the detection statistics could be performed without the need to assess cross- and slant-range performance, the latter was required to support hypothesis testing performed on image data to determine the impact of the PSA on the overall resolution of the system. In order to facilitate operational calibration of the baseline LADAR, it was necessary to both simulate and inject the signal at various points in the receiver. This was performed in several steps using the setup shown in Figure 2. To establish the detector coherent transfer function for a given total LO power and signal level at the balanced detector, the saturated output from the EDFA (manufactured by MPB) was split into LO and signal paths using a single-mode polarization-maintaining (PM) fiber splitter. Depending on the detector gain setting selected, the LO power level was then adjusted to give the desired output RMS shot noise voltage level. A programmable attenuator and fiber delay line in the signal path were then used to simulate the round-trip target range delay and signal levels expected to produce the full scale coherent detection current levels at the detector.

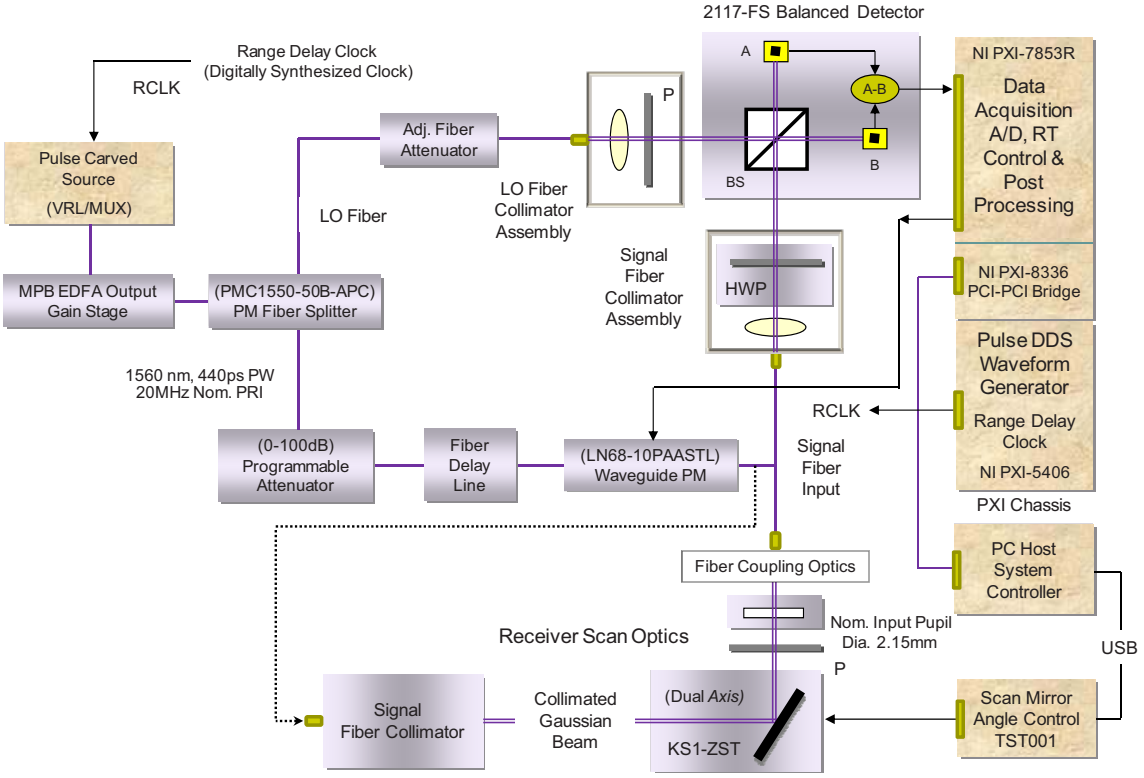

Figure 2. Baseline LADAR operational calibration setup.

Additionally, a waveguide phase modulator in the signal path was driven with a 50 kHz linear ramp voltage to produce a 2π phase shift every 20 μs. The resulting 50 kHz frequency-shifted optical signal drove the detected signal through all detection quadratures at a known rate. This approach provided an effective means for removing low-frequency system noise from the detection process, ensuring that normally distributed LO shot noise was the dominant noise source. Key to establishing the capabilities of the receiver involved an assessment of the overall noise performance predicted and measured for the detector, taking into account electrically generated detector readout noise and the optical shot noise contribution from the LO. Within the operational context of the receiver, the LO noise must dominate the detector electronic noise by a sufficient degree to ensure the detection statistics are truly LO shot-noise limited. Figure 3 shows the predicted and measured readout noise for the detector at the high differential current gain setting.

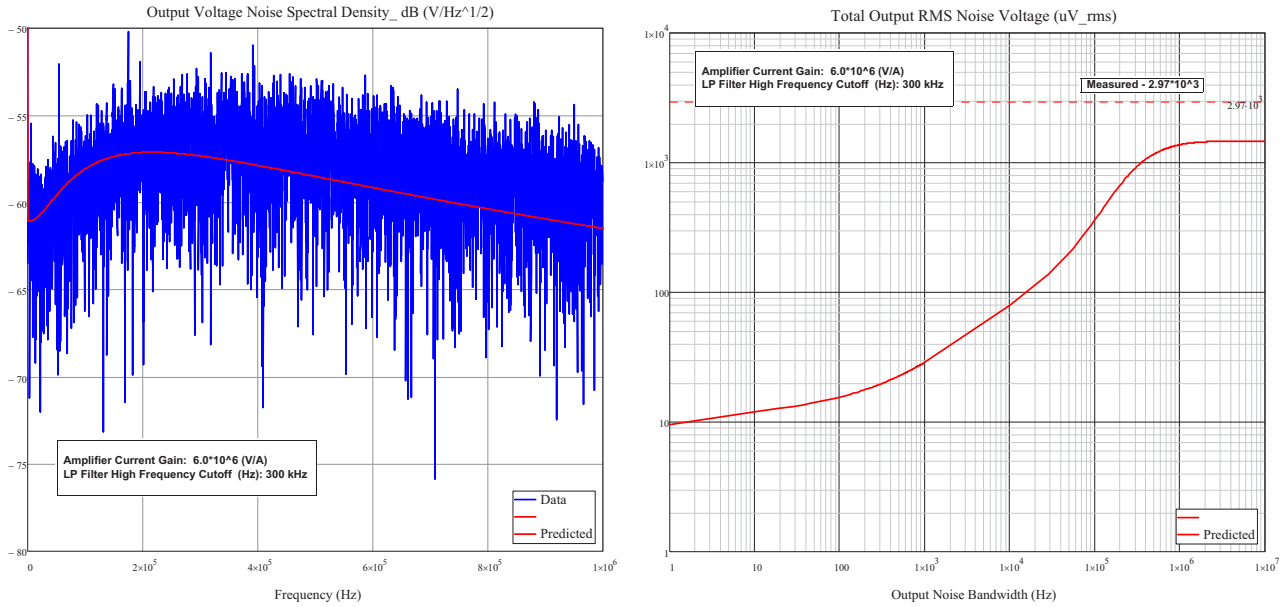

Figure 3. Balanced detector readout noise performance (high gain setting).

The significance of these are results are summarized in Figure 4, which shows the predicted and measured total RMS detector output noise, along with the relative magnitude of the LO shot noise contribution as a function of the mean LO photocurrent level. Here the value of the gain is adjusted slightly from the manufacturer's value, in order to fit the measured output noise data. These results indicate that for the high gain setting, the LO shot noise significantly dominates the detector readout noise for levels above 10 μW. The ability of the detection statistics to be accurately estimated by the 16-bit sampling A/D employed in the baseline LADAR processing platform, as well as measure changes in the dominant LO noise level when locking the gain quadrature of the PSA to the optimal balanced detection quadrature, was fundamental to demonstrating the impact of the PSA on the detection performance of the receiver.

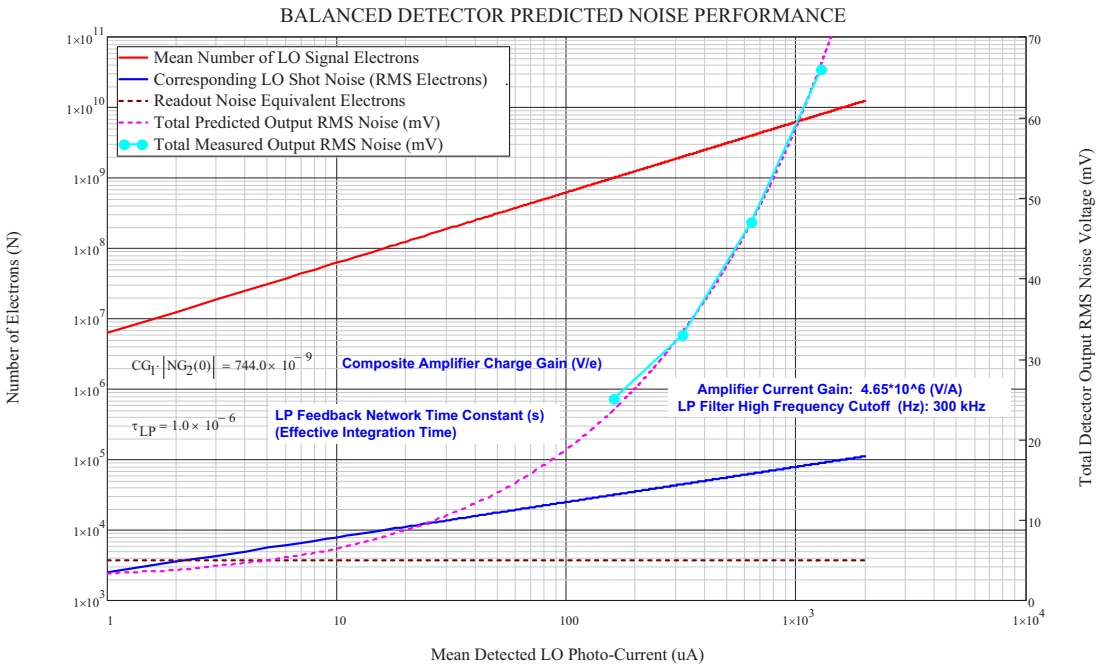

Figure 4. Magnitude of readout noise and LO shot noise (high gain setting).

2.2 Baseline LADAR Calibration

Using the calibration setup shown in Figure 2, detailed and precise measurements of the AC-coupled RMS output noise, coherent AC signal voltage, and corresponding harmonic spectral power, could easily be measured for a known average input power level associated with the pulse-carved signal pulse train. Figure 5.0 shows a typical measurement made at a detector output SNR of approximately 6.6 dB. Here an adjustable attenuator setting of 60 dB was used to produce an estimated optical signal power level of -92.5 dBm (0.57 pW) at the input to the detector. The optical signal was mixed with an LO having an optical power level slightly in excess of 200 μW producing an output 1 standard-deviation noise level of around 27 mV with no signal present. With the pulse width set to 440 ps, a Range Delay Clock (RCLK) setting of 22.12 MHz was used to temporally align the current LO pulse and delayed signal pulses emerging from the fiber delay line. The resulting coherent harmonic signal term is shown at the 50 kHz modulation rate in the presence of additive LO noise.

The detected signal could also be characterized in the frequency domain by specifying the modulo-two data acquisition buffer length used for FFT processing, along with the number of buffers (FFT's) to be summed and averaged in order to reduce the spectral noise variance. Results for the spectral noise power obtained for averaging 256 2^{14}-point FFTs on the collected data is shown in Figure 5 as well. Here the mean spectral noise floor power is reduced by a factor of 2^{13} or -39.1dB as a result of the FFT spectral filtering operation, while the spectral noise variance is further collapsed by a factor of (1/SQRT(256)) due to scalar averaging of the FFT results at each frequency.

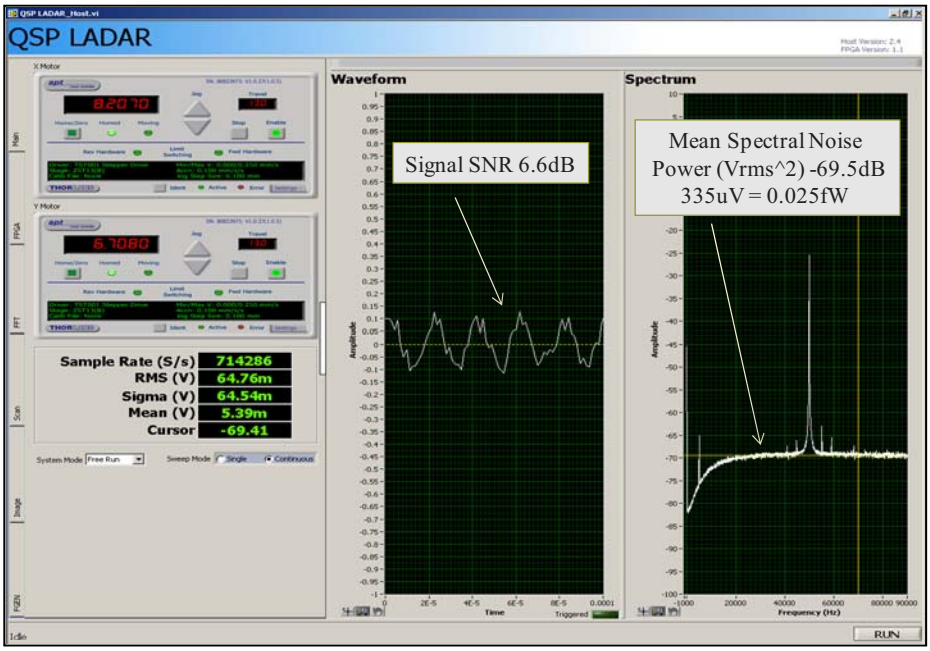

Figure 5. Detected coherent IF and spectral power.

In addition to establishing the detector coherent transfer gain for the baseline LADAR, the range resolution performance of the receiver was also characterized. Slant range is processed in the receiver as a result of a coherent matched filter operation produced by video integration of the coherent term resulting from pulse overlap between the LO and the return signal pulse. During the video integration period of approximately 1.0 μs, the phase of individual signal pulses varies only slightly during application of the 20 μs phase ramp to the transmitted signal beam, and charge resulting from coherent detection of a number of pulse returns is summed effectively by the detector. The relatively stationary phase relationship between the LO and received signal pulses during the video integration period produces a coherent signal sample of the 50 kHz offset applied to the transmitted beam.

Since the relative detected signal level is produced by varying the offset between the LO and signal return pulses, changing the clock rate applied to the pulse carver allows the receiver to essentially "walk" the LO pulse through the applicable range window with the desired resolution. These offsets are produced by varying the range delay clock (RCLK) frequency applied to the pulse carver using a precision COTS signal generator incorporating a 48-bit DDS

phase accumulator updated at a 100 MHz sample clock rate. A resulting detailed scan of the mean squared output voltage, which is proportional to the detected optical signal power, is shown in Figure 6 as a function of the slant range emulated by the calibration setup delay line. This scan is performed at large SNR to verify the expected resolution produced by the matched filtering operation alone. As expected the resolution obtained at half and one pulse width (PW) offset very closely matched the (c*PW_overlap/2) value that was anticipated for a PW of approximately 440 ps.

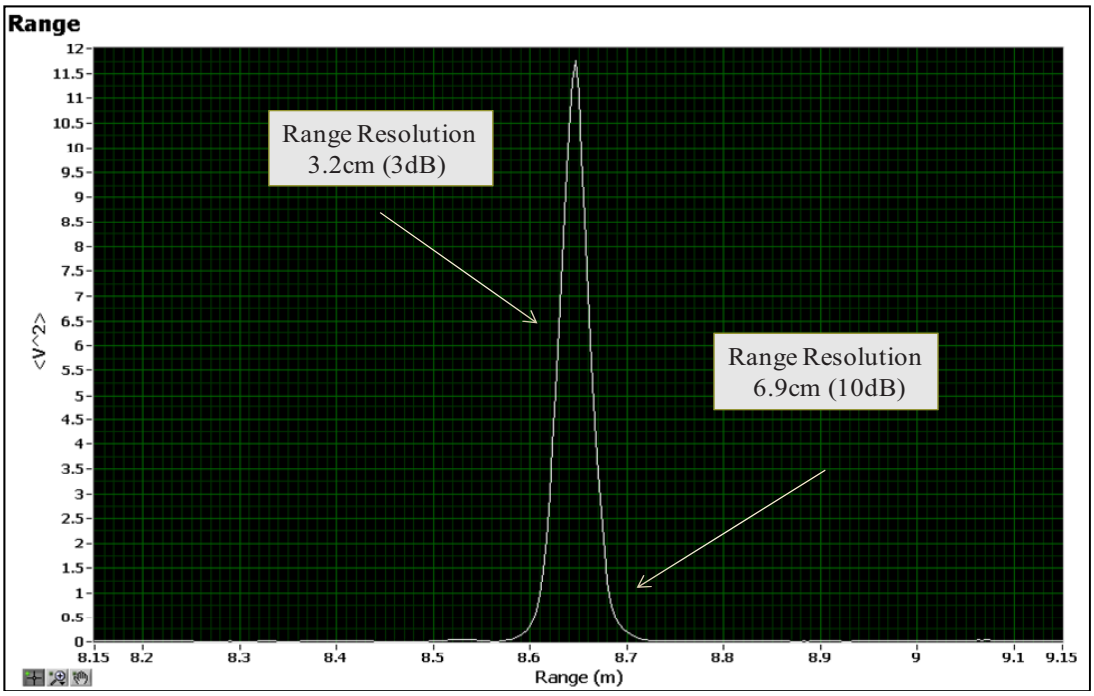

Figure 6. Baseline LADAR range resolution.

Inasmuch as jitter on the range delay clock serves only to place an uncertainty on the transmit pulse envelope, it does not affect the transmit pulse phase coherency between subsequent pulses and only needs to be bounded to a fraction of the pulse envelope in order to localize the target location. The output from all other signal returns are largely suppressed by the common mode rejection behavior exhibited by the balanced detector, and should introduce only a small error in the magnitude of the homodyne term.

Imaging systems in general may be characterized by their ability to resolve fine spatial detail inherent in the object being observed. All systems for which the amplitude of the light in the image plane can be represented as a superposition of individual PSF's (point spread functions) characteristic of the overall system optical impulse response, represent a linear convolution of the object's scattering profile with the system PSF. In general, the field in the image plane is a complex valued function, which depending on the degree of coherence present in the scattered field, may be treated as the superposition of real valued intensity functions associated with the system PSF. The inherent imaging "resolution" capability of the system in either case can still be inferred from the magnitude of the complex valued PSF. Exactly how the complex valued field in the image plane is manifest (i.e. the degree to which coherent speckle is present), and how this field is subsequently processed by the detection system, ultimately determines the degree to which the objects spatial information can be acquired.

In the current single-mode implementation of a coherent detection imaging baseline LADAR, calibration of the spatial resolution capability of the system was performed by providing a suitable optical plane wave which is directed to the input aperture of the receiver. This plane wave is produced by the signal fiber collimator shown in Figure 2. The receiver optics assembly shown in Figure 7 contains a dual-axis scan mirror to allow an image of an extended object to be generated sequentially in a raster scan process, varying the "look" angle across the object space of interest. Light

scattered from the target at each look angle is sequentially directed through an aperture before being collected and coupled to the receiver signal fiber for subsequent detection and processing.

In systems involving infinite conjugate imaging, as is the case here, it is more useful to think in terms of the angular resolution capabilities of the system. With knowledge of the object's range, angular information can easily be converted to a spatial coordinate description of the object's return.

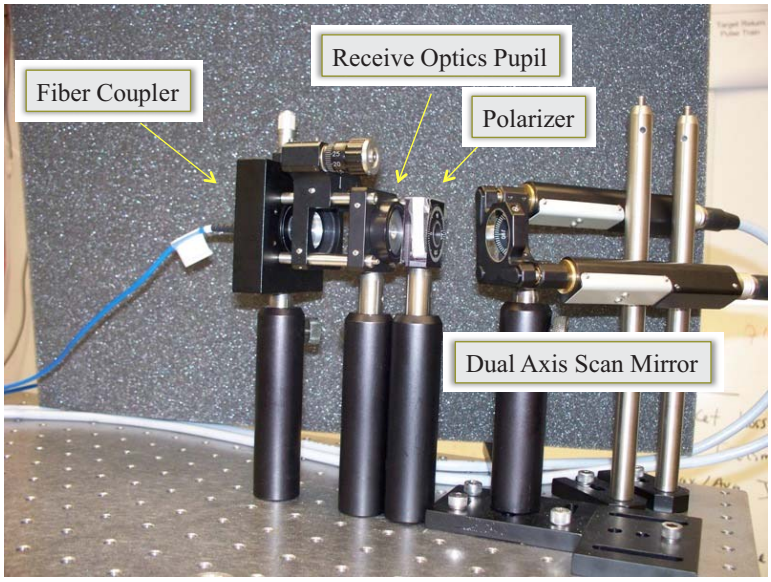

Figure 7. Baseline LADAR receiver scanning assembly.

The angle subtended in object space by the receive optics for any given setting of the scan mirror is determined by the inherent angular resolution of the receiver. In order to establish a reference resolution capability for the baseline LADAR, a circular aperture of known dimensions was placed at the input to the collection optics to establish the diffraction-limited pupil function for the receiver. The resulting angular resolution is easily determined from the known physical dimensions of the aperture and the wavelength of the illumination light. Implicit to imaging at infinite conjugate distances is the requirement for scattering points from the object to present a nearly uniform phase front across the input aperture.

In this case, the field amplitude produced at the focal plane of the coupling lens is then given by a two dimensional spatial Fourier transform of the complex amplitude of the light transmitted through the aperture. This distribution is given by the well known Airy function, and its relation in angle space may be mapped to a set of spatial coordinates in the transform plane of the lens by a simple scale factor given by the focal length of the lens. In addition, placing the aperture at the input focal plane of the lens produces a telecentric image at the transform plane, assuring rays mapped from the diffracted input field enter normal to the fiber end.

The resulting intensity distribution can then be measured directly using the calibrated angular transfer function for the input scanning mirror, and scanning the input mirror through the two dimensional angle range of the distribution. Figure 8 shows the measured angular intensity distribution out of the signal-coupled fiber for a nominally 2.15 mm-diameter circular input aperture as the scan mirror is moved over a +/-2 mrad field of view.

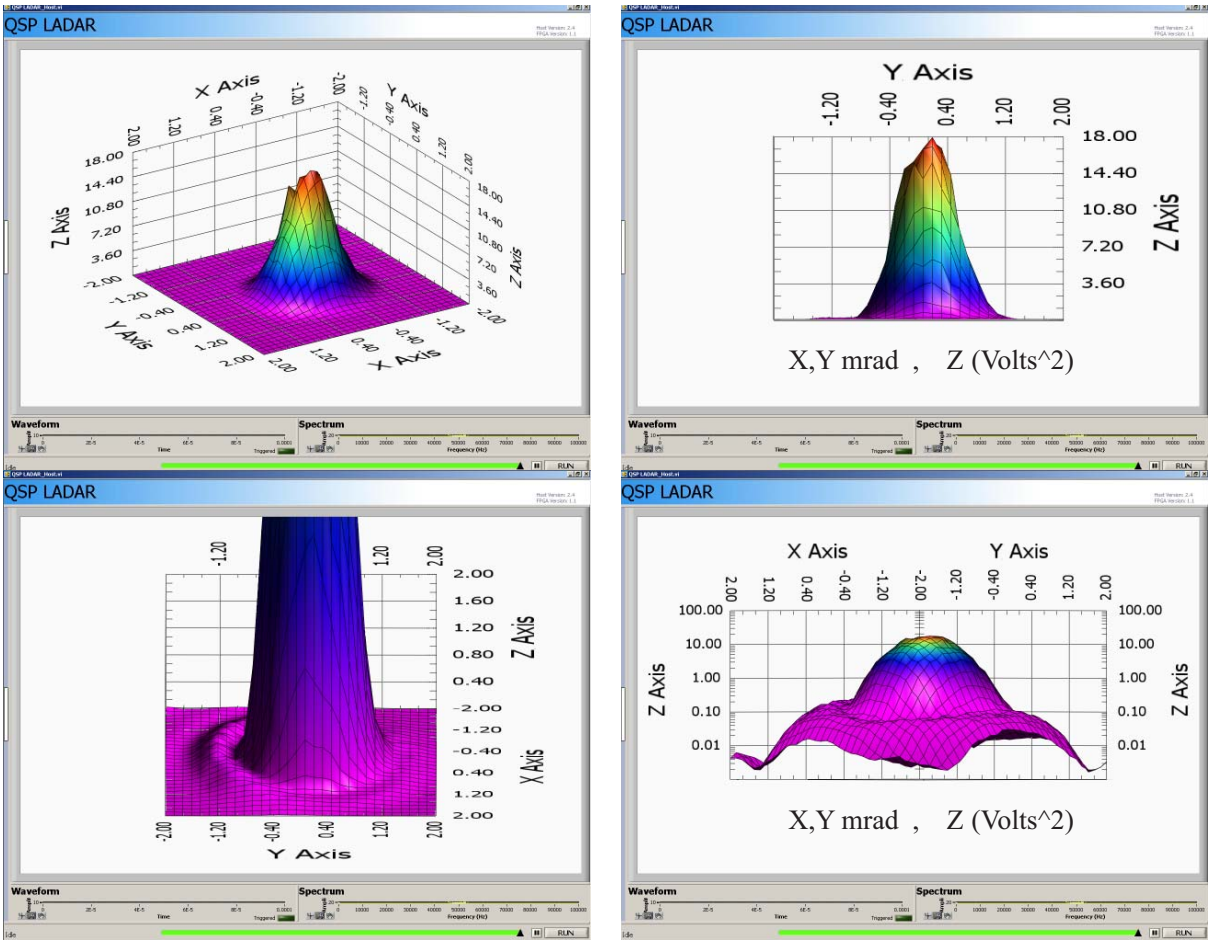

Figure 8. Baseline LADAR image resolution PSF – coherent detection 440 ps pulse.

With calibration of these critical LADAR performance parameters completed, standoff measurements were initiated by removing the programmable attenuator and fiber delay line from the calibration setup, and directing the signal output fiber to a separate target illumination collimator. Targets used for imaging were placed on a separate table within the QSP development laboratory. A diagram of the geometrical layout between the target location and the baseline LADAR scan mirror is shown in Figure 9.

A number of standoff coherent target images were produced using the baseline LADAR assembly during the current program phase. The image data was used to establish a set of baseline reference target geometries, which could be used to perform various hypothesis testing experiments in order to make quantitative assessment of the improvement in cross- and slant-range imaging possible by inclusion of either a PSA or a phase insensitive amplifier (PIA) in the signal detection path of the receiver. Hypothesis testing to determine "one" vs. "two" target scenarios under various SNR in the presence of highly developed speckle was performed as part of a collaborative activity in a separate effort.

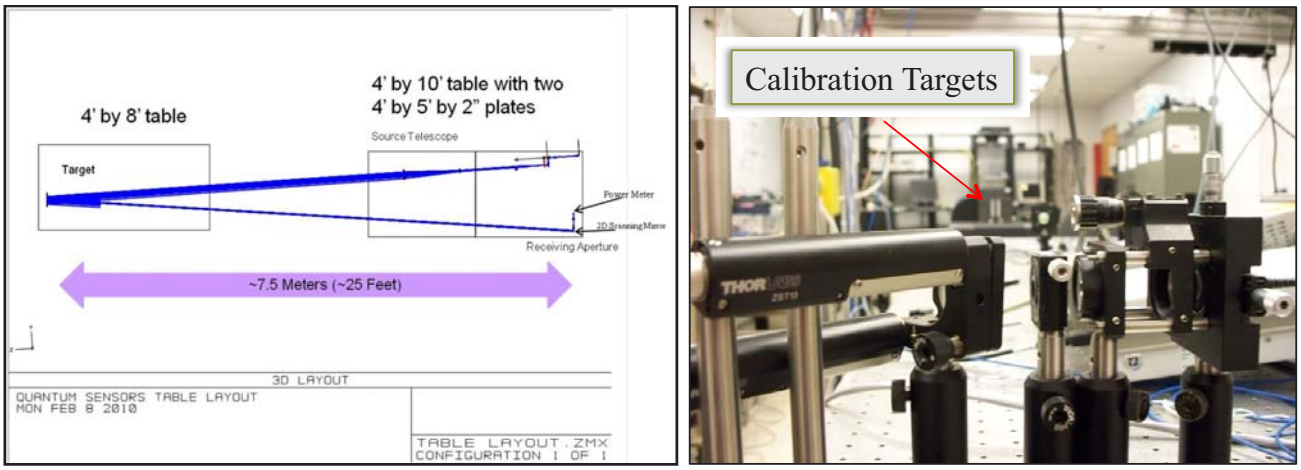

Figure 9. Target location in relation to baseline LADAR receiver.

Initial images were made at high SNR to mitigate the impact of receiver noise and establish the nature of the imaging with coherent speckle present. Figure 10 shows the coherent slant/cross range image made of the two aluminum rods with a paper overlay applied to the surface of the rods. The squared harmonic detector voltage, which is proportional to the received optical power, is plotted against the cross- and slant-range axes. Here, the slant range is stepped in 2.0 mm increments to obtain a high resolution measurement of the target distance at each receiver scan angle setting. The scan mirror is similarly stepped with a cross range sampling resolution of three samples/mrad, which is sufficient to obtain an adequate image given the PSF half-width for the LADAR receiver is on the order of 1.0 mrad. The polar range and cross range angle are then converted to linear Cartesian coordinates.

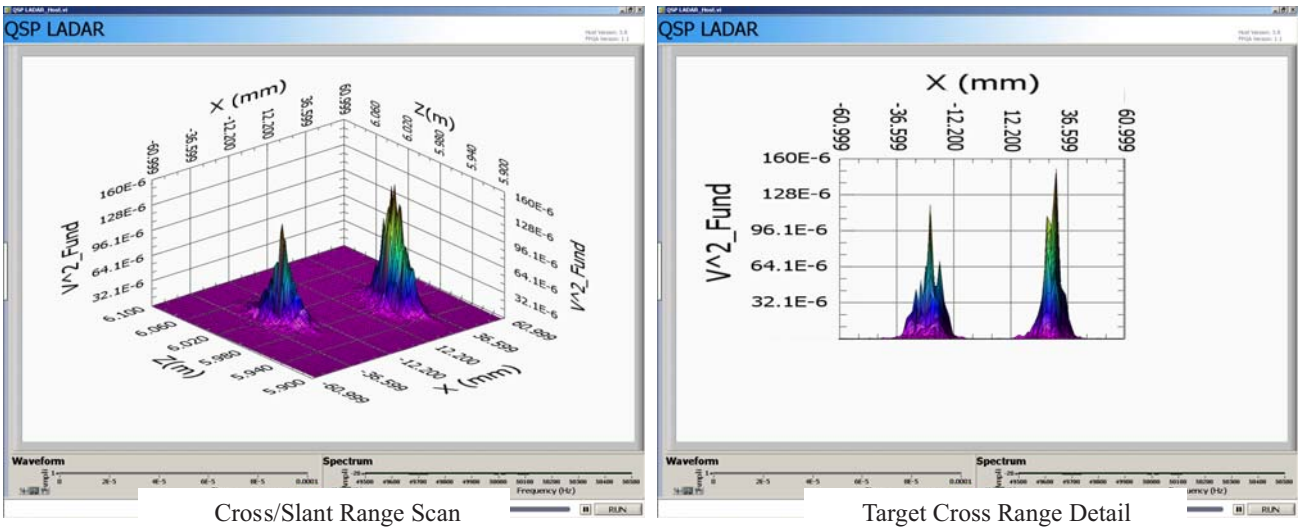

Cross/Slant Range Scan

Target Cross Range Detail

Figure 10. Baseline LADAR calibration target image scan.

In the next section, we address details related to the integration of the PSA into the baseline LADAR assembly, and discuss the impact on the detection noise statistics produced as a result.

3. BASELINE ENHANCEMENT WITH PHASE-SENSITIVE AMPLIFICATION

Phase-sensitive amplifiers have been shown to provide amplification with a noise figure lower than the 3-dB high-gain limit achievable in an ideal PIA[2,3]. This so-called 'noiseless' amplification provided by PSA allows for better SNR performance when using a PSA than a PIA. A PSA amplifies one quadrature of the input optical field while it de-

amplifies the orthogonal quadrature. Homodyne detection works well with PSA because it involves the detection of only one quadrature of the optical field. As long as the homodyne detector measures that quadrature that is amplified, a PSA can provide a noise figure close to 0 dB. A PSA can therefore provide up to a 3 dB SNR improvement over an ideal PIA with the same gain.

3.1 Implementation of phase-sensitive amplification

Figure 11 shows a block diagram of the layout of our optical system. To accomplish phase-sensitive amplification in our system, we require a 780 nm pump to be used in the parametric amplification process. To generate this pump, we first take a continuous wave 1560 nm laser with very long coherence length and carve it into short pulses (~400 ps in width, with a repetition rate of ~23 MHz). These pulses are passed through two amplification stages, at which point the average power at 1560 nm reaches 4 W, with peak power near 450 W. After amplification the pulses pass through a 10-mm-long second harmonic generating crystal made of periodically-poled Lithium Niobate (PPLN). This crystal converts approximately half of the 1560 nm light to 780 nm light in a frequency-doubling process.

To accomplish phase-sensitive amplification, we propagate the 780 nm pump beam through a 25-mm-long type 0 PPLN crystal along with the 1560 nm signal beam. This signal beam is the optical return scattered back toward the receiver from a target 7 m away from the receiver and illuminator. The signal and pump beams must be aligned properly in both the spatial and temporal domains to achieve amplification. A dichroic mirror combines the pump and signal beams prior to the PSA, aligning them spatially. Another dichroic mirror subsequently filters out the pump beam after it passes through the PSA. Both beams are focused in the center of the PPLN crystal. The pump has a circular waist with FWHM intensity of 27 μm, and the signal beam is also circular with a FWHM intensity of 40 μm^4. To achieve temporal alignment of the pump and signal beams, the optical path length traversed by LO pulses is set to exactly match the optical path length of the pump beam path. Because of this, when the pulse repetition frequency is tuned such that the signal and LO pulses (delayed by one pulse period relative to the signal) are temporally matched, the signal pulses automatically match temporally to the pump pulses for optimal amplification. After amplification, the signal beam is mixed with the LO and detected with a balanced detector.

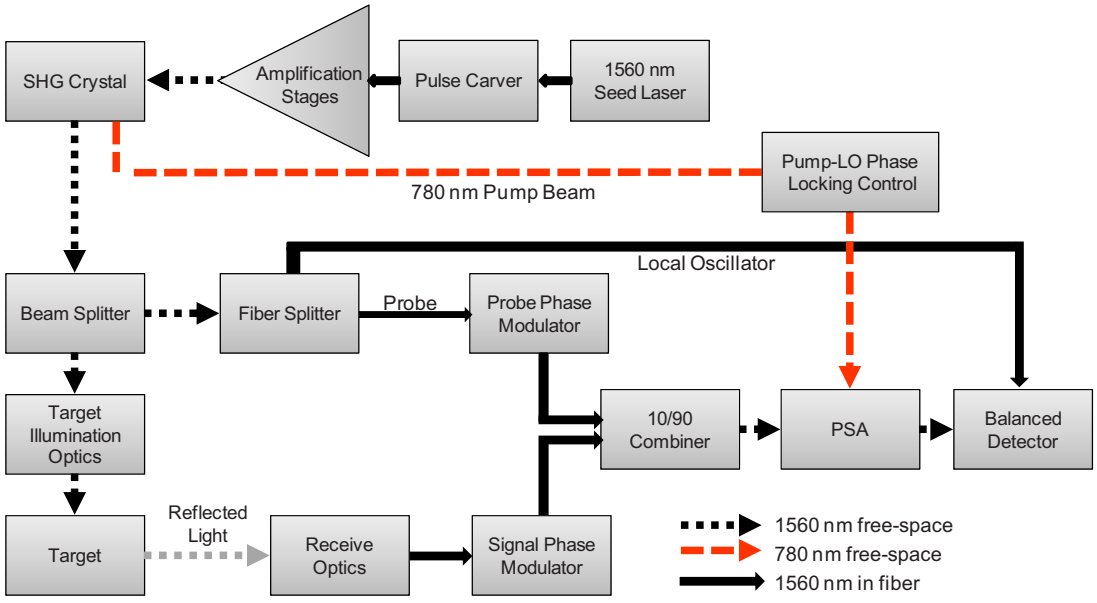

Figure 11. Block diagram of the PSA-enhanced LADAR system.

3.2 Phase-locking for optimal performance

Because the optical amplifier is phase-sensitive, only one quadrature of the signal return is amplified. Here the signal is frequency-shifted relative to the LO by 44.6 kHz (however, the pump beam is not frequency shifted, so it oscillates at exactly twice the optical frequency of the LO). This frequency shift causes the signal to cycle in and out of phase with the LO, resulting in a sinusoidal output voltage from the balanced detector. The output voltage is sampled and those

samples are Fourier-transformed and a power spectrum is taken. The signature of the signal is an isolated peak in the power spectrum at 44.6 kHz, whose value is proportional to the optical power in the signal return. This frequency shift also causes the signal return to be alternately amplified and deamplified as it cycles in and out of phase with the pump beam. Since the signal is amplified whenever its phase relative to the pump at the input to the PPLN crystal is either 0 or π, the signal goes through amplification (and deamplification) two times during each cycle of the 44.6 kHz oscillation.

To optimally detect the amplification of the signal, these amplification events must be in phase with the LO[5]. In other words, optimal detection occurs when the pump and LO phases are locked together in a specific relationship. Due to random small drifts in temperature and mechanical positioning of the table and optics on it, this phase relationship does not remain constant. If the phase relationship is optimal at one point in time, a drift of 90° in the phase of the LO and pump beams relative to each other results in the balanced detector only seeing the deamplified quadrature of the signal, significantly decreasing performance. A means of actively locking the pump and LO phases together is the only way to ensure the best performance of the LADAR.

Because the pump and the LO don't interact directly, their relative phases cannot be measured directly. Also, since the signal is random in phase and amplitude, it cannot be used to reliably measure the pump-LO phase. We therefore developed the concept of using a 'probe' beam to lock the pump and LO phases together. Figure 11 shows a block diagram of the setup, in which we split the 1560 nm light that is not used to illuminate the target into two parts – the LO and the probe. The probe beam's optical path is matched in length to the LO path. We use a phase modulator to frequency-shift the probe beam relative to the LO by 9.76 kHz, causing the probe to cycle in and out of phase with the LO at that frequency. The probe beam is combined with the signal beam using a 90/10 fiber splitter and from then on it has a common path with the signal. The power in the probe beam is measured by taking the value at 9.76 kHz from the power spectrum. With the PSA and signal off (i.e., with the pump and target illumination beams blocked), the power measured in the probe is steady. When the PSA is turned on, the probe power (in the spectral domain) begins to fluctuate as the LO alternately measures the amplified and deamplified quadratures due to drifts in the relative phase between the LO and pump.

By keeping the probe power (in the power spectrum domain) maximized, we guarantee that the pump-LO phase is such that the LO is interrogating only the amplified quadrature of the probe. The probe and signal beams have a common path from the PSA to the balanced detector, and differ in optical frequency by only a very small amount (35 kHz). This means that if the probe power is held at its maximum, the detection of the signal beam will also be maximized, because the pump-LO phase is independent of any signals passing through the PSA. If one signal passing through the PSA and measured with the balanced detector is maximized, the pump-LO phase is optimal; and all other signals following the same path will also be maximized (optimally detected).

To keep the probe power maximized, we apply a small sinusoidal dither (at ~30 Hz) to the phase of the pump beam. This dither causes the probe power (in the power spectrum domain) to fluctuate in a periodic manner. We derive an error signal by multiplying this fluctuating power level by a sinusoid at the same frequency and phase as the dither, then integrating the result over an integer number of periods. This approach gives a signed error signal which tells us in which direction to adjust the bias to the pump beam's phase in order to compensate for drift. This pump-LO phase locking system has proven to work well and to maintain a high degree of phase-locking for extended periods of time.

Figure 12 shows a schematic diagram of the pump-LO phase-locking setup. The input to the system (shown at lower left) is split into two parts – the LO and the probe beams. The probe beam is frequency shifted relative to the LO by 9.76 kHz, then combined with the signal return (10% loss on signal, 90% loss on the probe) and passed through the nonlinear crystal, where it is amplified. The probe is then detected by the balanced detector and a power spectrum is generated, which peaks at the frequency by which the probe is offset from the LO. A sinusoidal pump phase dither is applied by driving a PZT mirror in the path of the pump. The dither results in a periodic modulation of the detected spectral domain power in the probe beam. A plot of the power spectrum is also shown in Figure 12. Demodulation allows the generation of an error term which is used for feedback to adjust the bias phase to maintain phase locking. Keeping the spectral power in the probe beam maximized ensures optimal performance of the LADAR receiver.

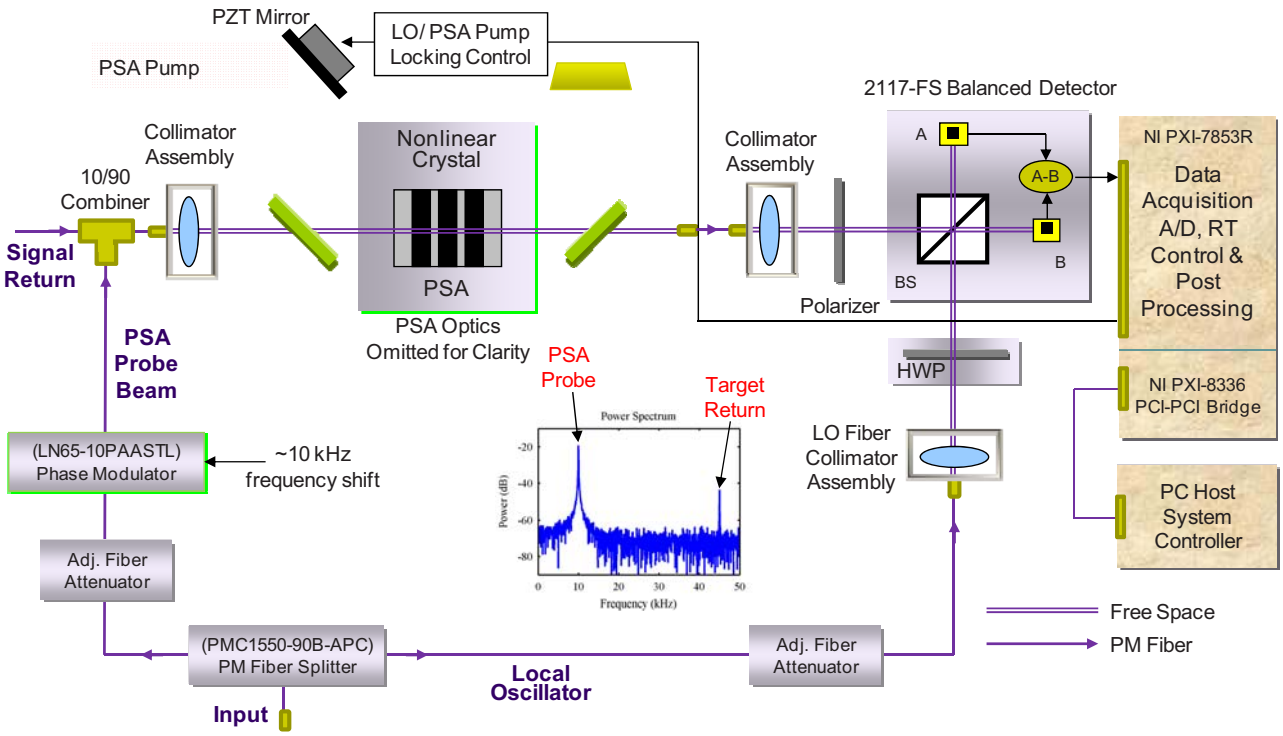

Figure 12. Diagram of the important components used in maintaining phase-locking of the pump and LO.

4. EXPERIMENTAL RESULTS

Experiments with the PSA-enhanced LADAR showed that it achieves a level of performance that cannot be realized with a PIA. The simplest scenario for demonstrating the performance improvements afforded by the PSA over a PIA involves using a specular target. In this case, we can perform a simple hypothesis test to determine from the returned signal whether or not a target is present[6], and from this test derive a receiver operating characteristic (ROC).

4.1 Target detection statistics

A standard hypothesis test to characterize a receiver is to measure how well the receiver discriminates between cases of a single target being present or not. To this end, we take data with and without a target present, and with and without the PSA turned on. Comparing the no-PSA no-target data to the no-PSA, target-present data allows us to quantify the performance of the baseline system, with no amplification. To generate ROC curves, we perform a simple threshold test in which we take 10,000 data samples for each case of the target being present or not. Each data sample represents the power-spectrum value of the voltage in the frequency bin where our signal is located (44.6 kHz), with the power spectrum being generated from an FFT of 2^n time-domain voltage samples from the balanced detector. We then set a threshold voltage at a certain level. For the target-present samples, the fraction of the samples above this threshold constitutes the probability of detection. For the no-target data, the fraction of these samples above the threshold constitutes the probability of false alarm. Probability of detection can then be plotted against probability of false alarm for a number of different threshold values to generate an ROC curve.

The distributions of the measured data samples show clearly how the no-target data points (the noise) and the target-present (signal plus noise) data points change when the PSA is turned on. Normalized histograms of the data with no target present, displayed in Figure 13 on the left, show good fit to the expected exponential distributions (the smooth curves)[7,8]. Data for the PIA case has not yet been taken, but simulated curves are for an ideal PIA with 3 dB noise figure in the high-gain limit are also shown.

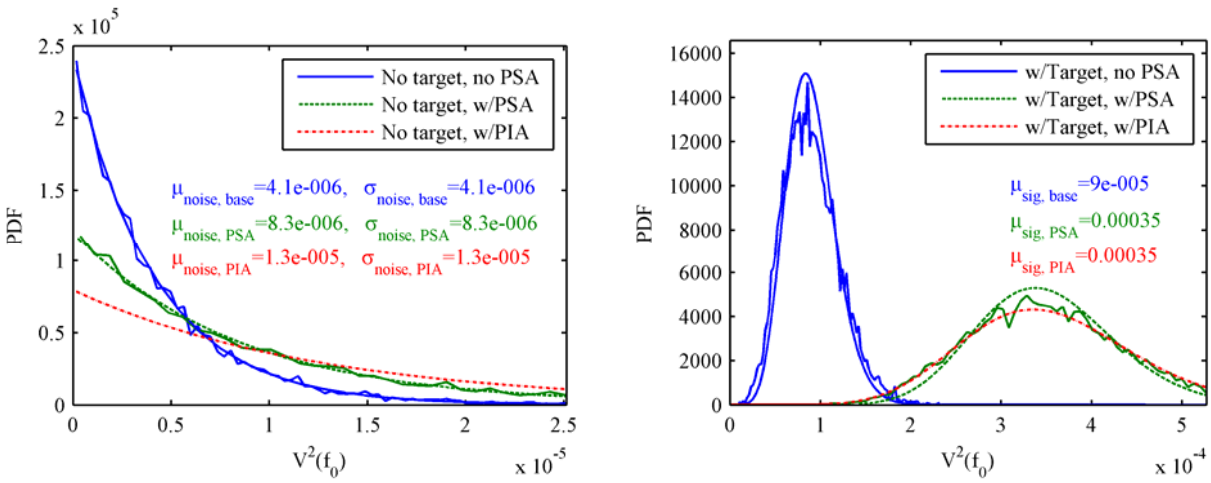

Figure 13. Theoretical probability density functions (smooth curves) and normalized histograms of data points (rough curves) with no target present (left) and with a target present (right).

The zero-mean, normally distributed, time-domain noise voltage samples obtained from the balanced detector have a variance of σ_{TD}^2. With LO shot noise being the dominant noise source, the mean and standard deviation in the power spectrum, μ_0 and σ_0 respectively, are given by[9]

$$\mu_0 = \frac{2\sigma_{TD}^2}{N}, \text{ and } \sigma_0 = \frac{2\sigma_{TD}^2}{N}\sqrt{\frac{N+1}{N}}, \tag{1}$$

where N is the number of points (frequency bins) in the power spectrum. The data sets used in Figure 13 use N=512. When amplification is provided, the standard deviation of the noise in the power spectrum for PSA and PIA changes according to the following relations[7,8]

$$\sigma_{PSA} = \sigma_0[\eta(G_{eff} - 1) + 1], \sigma_{PIA} = \sigma_0[2\eta(G - 1) + 1], \tag{2}$$

where G_{eff} is the effective gain of the PSA (gain of the amplified quadrature), G is the gain of the PIA, and η is the overall detection efficiency, which includes losses downstream of the amplifier, signal-LO mixing efficiency, and detector quantum efficiency.

With a target present, we get the normalized histograms and theoretical distributions shown on the right in Figure 13. When the PSA is turned on, the data in the left plot shows that the noise increases significantly compared to the unamplified case. The signal also increases by a large amount (right plot). The measured gain with the PSA turned on is 6 dB. The inferred detection efficiency, η, is 0.345, which is close to the measured value of around 0.3. Note that each of the 10,000 data points is taken from a single power spectrum having 512 points. The data obtained for the PSA as shown in Figure 13 shows good agreement with theoretically predicted distributions.

4.2 Signal-to-noise ratio enhancement

SNR is defined by the following relation:

$$SNR = \frac{\mu_{sig} - \mu_{noise}}{\sigma_{noise}}, \tag{3}$$

where μ_{sig} is the mean value of the data samples with signal present, μ_{noise} is the mean with no signal present, and σ_{noise} is the standard deviation with no signal present. All of these values are computed from the spectral-domain data. The data plotted in Figure 13 show that the SNR in each case is 13.2 dB for no amplification, 16.1 dB for the PSA case, and 14.3 dB for the ideal PIA case (assuming the same gain as for the PSA). Note that for the same level of amplification (G_{eff} = G = 6 dB), the PSA provides a larger improvement in SNR than the ideal PIA. This result agrees with simulations of the SNR vs. detection efficiency shown in Figure 14. The plot shows theoretical curves representing a baseline system with no amplification compared to a PSA-enhanced system and an ideal PIA-enhanced system.

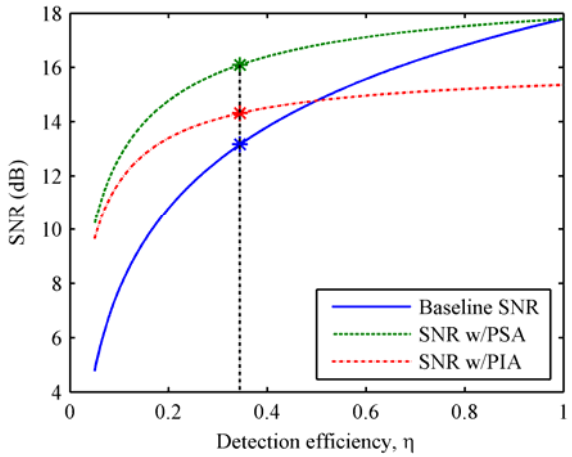

Figure 14. Simulation of SNR vs. detection efficiency for unamplified and amplified coherent receivers.

The SNR in the three cases plotted in Figure 14 are given by the relations[10]

$$SNR_{baseline} = 2\eta N_s$$
$$SNR_{PSA} = \frac{2\eta G_{eff} N_s}{\eta(G_{eff}-1)+1}, \quad (4)$$
$$SNR_{PIA} = \frac{2\eta G N_s}{2\eta(G-1)+1}$$

where N_s is the signal photon number. The asterisks show the SNR values at the inferred value of η, 0.345. These points agree very well with the measured data from Figure 13. For this particular simulation, G_{eff} and G are both 6 dB, and the input photon number is 30. The plot also shows that there is a fairly broad range over which a PSA can provide a significant advantage over an ideal PIA for a shot-noise-limited coherent detection system. Figure 14 shows that a PSA can compensate for more effectively than a PIA for any losses incurred in the coherent detection process, such as in coupling to the interferometer, in mixing efficiency, and in quantum efficiency.

5. SUMMARY

This work represents the first quantum-enhanced LADAR showing performance improvement above that achievable using a classical LADAR sensor. This improvement is enabled by phase-sensitive amplification of the return signal from a standoff target, and coherent detection of that signal with phase locking of the PSA pump and LO. We have described a baseline coherent LADAR against which improvements are quantified and have shown good agreement between theoretically predicted performance and experiment with a simple hypothesis test. Future work will include experimental demonstration of the superior performance of a PSA over a PIA.

ACKNOWLEDGEMENTS

This material is based upon work funded by DARPA's Quantum Sensor Program, under AFRL Contract No. FA8750-09-C-0194. Any opinions, findings and conclusions or recommendations expressed in this material are those of the author(s) and do not necessarily reflect the views of DARPA or the United States Air Force.

REFERENCES

[1] Dutton, Z., Shapiro, J. H. and Guha, S., "LADAR resolution improvement using receivers enhanced with squeezed-vacuum injection and phase-sensitive amplification," J. Opt. Soc. Am. B 27, A63-A72 (2010).

[2] Caves, C. M., "Quantum limits on noise in linear amplifiers," Phys. Rev. D 26, 1817-1839 (1982).
[3] Levenson, J. A., Abram, I. and Rivera, T., "Reduction of quantum noise in optical parametric amplification," J. Opt. Soc. Am. B 10, 2233-2238 (1993).
[4] Bhagwat, A. R., Alon, G., Lim, O., Chen, C., Kumar, P., Annamalai, M. and Vasilyev, M., "Generation and verification of traveling-wave phase-sensitive eigenmodes of an optical parametric amplifier," CLEO 2011, QThN4 (2011).
[5] Smith, K. H., "Method of locking a local oscillator to the amplified quadrature of a phase-sensitive amplifier," Internal Memorandum, 2011.
[6] Van Trees, H. L., [Detection, Estimation, and Modulation Theory: Part I], John Wiley & Sons, Inc., New York, 23-46 (1968).
[7] Shapiro, J. H., "On the statistics of noise, signal-plus-noise, and target detection for a specular target," Internal Memorandum, 2011.
[8] Shapiro, J. H., "On the statistics of noise, signal-plus-noise, and target detection for a specular target: part II," Internal Memorandum, 2011.
[9] Smith, K. H., "Signal phase modulation and spectral shot noise statistics in the Harris QSP balanced homodyne LADAR," Internal Memorandum, 2011.
[10] Glasser, R. T., "The Harris LADAR testbed and its compatibility with PSA and PIA," Internal Memorandum, 2011.